Chapter 2

Oil-Spill Pollution
Remote Sensing by Synthetic Aperture Radar

Yuanzhi Zhang, Yu Li and Hui Lin

Additional information is available at the end of the chapter

http://dx.doi.org/10.5772/57477

1. Introduction

Oil-spill, one of the major marine ecological disasters, can result in enormous damage to the marine environment and great difficulties to clean-up operations. In 2002, oil leaked from the sunken tanker Prestige off the coast of Galicia, polluted thousands of kilometers' coastline. In April 2010, the explosion of British Petrol's drilling rig Deepwater Horizion (DWH) in Mexico Gulf caused the largest accidental oil-spill throughout history. During 87 days of oil leaking from a sea–floor gusher, approximately 780,000 m^3 of oil, methane or other petro products was flowed into the Atlantic Ocean. In 2011, Bohai Sea, oil-spill was caused by the crack of submarine fault, triggered by the over pressure caused by oil extraction operation of Conocophillips Petro, China. Approximately 700 barrels of crude oil was leaked into the sea, and there were also about 2500 barrels of mineral oil-based mud deposited on the sea bed. Besides, a large proportion of oil-spills were caused by deliberate discharges form tankers or cargos, for the reason that there are still some vessels used to clean their tanks or engines before entering into the harbor. All these accidents and illegal acts caused huge damage to the costal ecosystem and marine environment. As a result, early warning of oil-spill accidents by remote sensing is very important for costal environmental protection and has become a vital task for maritime surveillance.

Optical sensors can be used for the application of oil-spill detection, however they are unavoidably suffered from weather and light conditions. For example during the Qingdao oil pipe accident that took place in Nov. 2013, crude oil flowed into the bay through drainage channel. Heavy smoke caused by the explosion covered the whole scene, which largely hampers the application of optical based sensors. Moreover there are also a lot of oil-spill accidents takes place during night or stormy weather. Due to its advantage of wide areal coverage under all-weather conditions the imaging capability during day-night times (Gade

and Alpers, 1999), satellite synthetic aperture radar (SAR) data from ERS-1/2, ENVISAT, ALOS, RADARSAT-1/2, and TerraSAR-X have been widely used to detect and monitor oil-spill (e.g., Alpers & Espedal, 2004a; Migliaccio *et al.*, 2007 & 2009; Topouzelis et al., 2008 & 2009; Marghany & Hashim, 2011; Zhang et al., 2012). Airborne SAR sensors like Uninhabited Aerial Vehicle Synthetic Aperture Radar (UAVSAR, by JPL, L-band) and E-SAR, (by DLR, multi-land) have also proven their potential for scientific research of marine or land remote sensing. With a series of key breakthroughs of SAR remote sensing technology, especially the multi-polarimetric capability and increased resolution, oil-spill detection by SAR has become a very hot research area (Solberg, 2012).

Based on basic principles of marine SAR remote sensing, this chapter will discuss state-of-the-art technologies of SAR oil-spill detection, and introduce several ways of investigating the environmental impact of oil pollution to costal environment. Several new trends within or beyond current applications, which will improve the performance of SAR oil-spill detection and provide more concrete information for studies in the near future, will also be introduced.

2. Basic principles of SAR oil-spill detection

SAR is an active radio equipment which transmit microwave and record the signal scattered by the target. The main mechanism of SAR marine remote sensing is observing the interaction between microwave and short-gravity and capillary waves of the sea surface. The backscattered signal from the sea surface can be described by backscattering coefficient σ^0, which stands for the uniformed radar cross-section.

At small incidence angle (<20°), the curvature radius are large enough compared with the wavelength of radar signal, specular scattering can be used to describe the scattering process and σ^0 can be solved by Kirchhoff approximation. At middle and large incidence angle (>30°), the backscattered signal is dominated by Bragg scattering:

$$\lambda_B = \frac{\lambda_r}{2\sin\theta} \tag{1}$$

where λ_B stands for the wavelength of Bragg scattering, λ_r stands for the wavelength of radar signal, θ stands for the incidence angle. Currently small perturbation model (SPM) is always used for calculating the scatter coefficient caused by Bragg scattering.

According to the composite sea surface model, the roughness of sea surface can be seen as small scale capillary waves superimposed on large scale grave waves (Fig. 1). So the backscattered radar signal can be treated as Bragg scattering modulated by the tilted scattering surface caused by large scale gravity waves. In mathematic expression, there are:

$$\sigma_0 = \sigma_0^S + \sigma_0^B \tag{2}$$

http://dx.doi.org/10.5772/57477

where σ_0^S and σ_0^B stand for backscatter coefficient calculated by model of specular and Bragg scattering respectively.

Since ancient Greek, physicists have noticed the damping effect of spilled oil films on the rough sea surface (Aristotle, Problematica Physica). Besides, some experienced sailors knew that pour oil to the sea surface could reduce the turbulence of sea surface and used this method to avoid ships from sinking in stormy seas. However systematic theory was not established to explain this phenomenon until Italian scientist Marangoni (Marangoni, 1872) pointed out that matter with different viscosity presents on the surface of fluid will produce elastic resistance to the movement of the surface, hence reduce the surface wave intensity.

The damping of oil films on the short-gravity and capillary waves can be measured by the ratio between backscatter coefficients of oil covered area and background sea surface. It is worth noting that the detectability of oil-spill by SAR relies closely on the wind speed above sea surface: if the sea surface wind speed is too slow, sea wave cannot be well developed and if it is too large, spills will break and be dispersed by mixing with seawater. So normally the ideal wind speed for oil spill detection is between 3m/s to 14m/s.

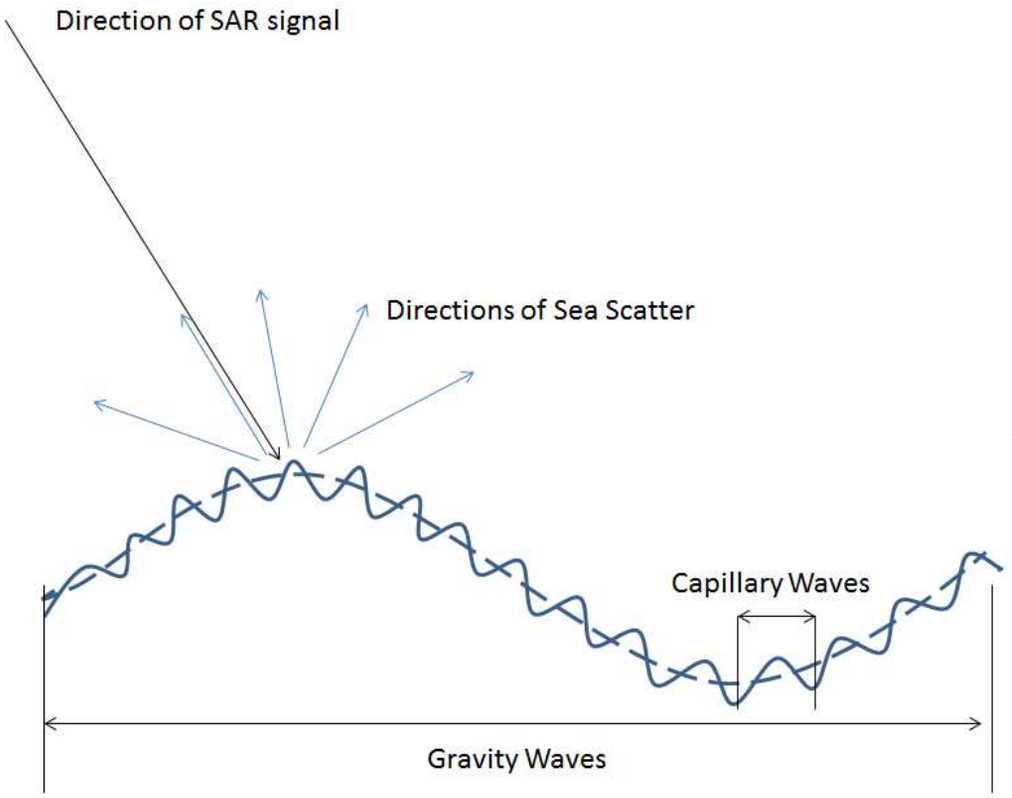

Figure 1. Demonstration of radar signal scattering from sea surface.

3. SAR Sensors and systems for oil-spill detection

Table 1 lists several main spaceborne SAR platforms. It can be found that multi-polarimetric capability has become a trend of advanced SAR satellites nowadays. And a series of SAR satellites constellations in plan will provide shorter revisit time for maritime monitoring in the near future. Discussion on the optimum frequency and polarization for SAR oil-spill detection can refer to Solberg's (2012) and other people's studies. Generally speaking, VV polarization performs better in highlighting oil slicks from sea background for stronger power return, however it may vary according to different oil types and sea conditions.

Sensors	Frequency	Polarization	Resolution*[1]	Swath width*[1]	Revisit/Repeat time*[3]
ERS 1/2 (Not operational)	5.3 GHz (C-band)	VV	4*20 m	80~100 km	35 d (Repeat)
Radarsar-1 (Not operational)	5.3 GHz (C-band)	HH	8~100m	50~500 km	2/24 d
Envisat-ASAR (Not operational)	5.331 GHz (C-band)	HH/HV; VV/VH; VV/HH	4*20, 150m	100, 400 km	2~3/35d
ALOS PALSAR (Not operational)	1.27 GHz (L-band)	HH, HV, VH, VV	7~100m	20~350 km	2 /46 d
TerraSAR-X	9.65 GHz (X-band)	HH, HV, VH, VV	1~16m	5~100 km	2 /11d
Radarsat-2	5.4 GHz (C-band)	HH, HV, VH, VV	3~100m	20~500 km	1/24d
Cosmo-SkyMed Constellation	9.6 GHz (X-band)	HH/HV; VV/VH; VV/HH	1~100m	10 km	1/16 d
HJ-1C SAR Constellation (1 /4)*[2]	3.2 GHz (S-band)	VV	5~20m	40,100 km	1/4d
Sentinel-1 Constellation (2 In plan)	5.4 GHz (C-band)	HH;VV; HH/HV; VV/VH;	5~20m	80,250,400 km	1~3/12d (6d with two satellites)
ALOS-2 (In plan)	1.3 GHz (L-band)	HH, HV, VH, VV	1~100m	25~490 km	14 d (Repeat)

*[1]Resolution (approximate) and swath width may vary with operation modes;

*[2]In operation/Total planed;

*[3]Revisit time (general): revisit at different incidence angle; Repeat time: orbit revisit, applicable for InSAR.

Table 1. List of main spaceborne SAR sensors that can be used for oil pollution monitoring.

http://dx.doi.org/10.5772/57477

Airborne SAR sensors are also useful for quick respond of oil-spill accidences. The Uninhabited Aerial Vehicle Synthetic Aperture Radar (UAVSAR), designed by Jet Propulsion Laboratory (JPL) at California Institute of Technology, US, is a reconfigurable, polarimetric L-band synthetic aperture radar with a 22-km-wide ground swath at 22° to 65° incidence angles. At present stage it is mounted beneath a Gulfstream III jet for experimental missions. The sensor has shown great performance in studies of land deformations, vegetation, ice & glaciers, and of course, oceanography. E-SAR is an airborne experimental SAR system operated by the German Space Agency (DLR). Since delivered its first images in 1988, the system has been continuously upgraded to become a multi-band and multi-polarimetric SAR sensor for a variety of Earth observation applications. In 2011, China successfully developed airborne multi-band, multi-polarimetric SAR interferometric mapping system, which includes radar systems and platform, data processing & mapping software and data distributing system.

There are several oil-spill monitoring systems in operation, among which CleanSeaNet satellite monitoring service is probably of the most famous one. It was set up and operated by the European Maritime Safety Agency (EMSA) since April 2007 and has developed to its 2nd generation. It takes advantage of images from a series of SAR and optical sensors. Together with auxiliary information such as meteorological and oceanographic data, the service could detect and report oil-spill accidents in near real time. Canadian Ice Service launched another real-time operational program called ISTOP (Integrated Satellite Tracking of Pollution), which uses the RADARSAT-1 data to monitor ocean and lakes for oil slicks and tracking the polluters (Gauthier, 2007). Some software have also been developed such as semi-automatic SAR oil-spill detection system developed by Konsberg Satellite Services, Norway, and Ocean Monitoring Workstation developed by Satlantic Inc. Canada. State Oceanic Administration of China also developed SAR satellites based oil-spill monitoring system and used it to regularly monitor Bohai Sea since 2009.

4. SAR automatic oil-spill detection algorithms

Synthetic Aperture Radar is an active microwave remote sensing device, which takes advantage of relative motion between its antenna and the target to achieve higher spatial resolution. As mentioned before, the oil-covered region appears smoother than its surrounding sea surface. In other words, the Bragg scattering in these areas is weakened. And in SAR image this phenomenon is usually observed as dark patches. However, in SAR images, the backscattered signal from oil-spill are very similar to the values of the backscattering from calm sea areas and other ocean phenomena called “look-alikes”. In the following part, explanation and examples of some main look-alikes are provided:

Low wind area: area where the surface wind is very slow (<2m), such as areas sheltered by land. Low wind swayed sea surface acts just like a mirror, which reflect most radar signal to the opposite direction of the receiving antenna. So they are observed as low backscattered area.

Biogenic films: natural films produced by phytoplankton and fishes are commonly found on the sea surface. Most of them are a very thin layer of surfactants with one to several molecules,

which reduces the surface tension dramatically. As a result, they are always observed as dark area.

Rain cells: also known as convective rain, which is the common form of rain in the tropics and subtropics (Alpers, 2004b). The typical structure of rain cell has downdraft as its core with circular gust front surrounded. The gust front will produce strong wind and always increase the sea roughness while the downdraft sometimes dampens the Bragg waves in form of precipitation. So some rain cells may have the signature of a darker core with much brighter surroundings compared with surrounded sea surface in SAR images (Alpers, 2004b).

Oceanic Internal Waves (OIW) and Atmospheric Gravity Waves (AGW): both of them have linear structures with bright and dark strips appear alternatively in SAR images. They can be distinguished based on solitary wave and radar imaging theories (Alpers et al. 2011).

Besides, ocean physical phenomena such as grease ice and upwelling zones may also cause dark spots or zone in SAR images. Together with a stripe-like oil-slick, typical images of the above-mentioned look-alikes are provided in Fig. 2. However, in a lot of cases, their characteristics such as shape or texture may be very close to each other, which makes them very difficult to be distinguished using any simple criteria alone.

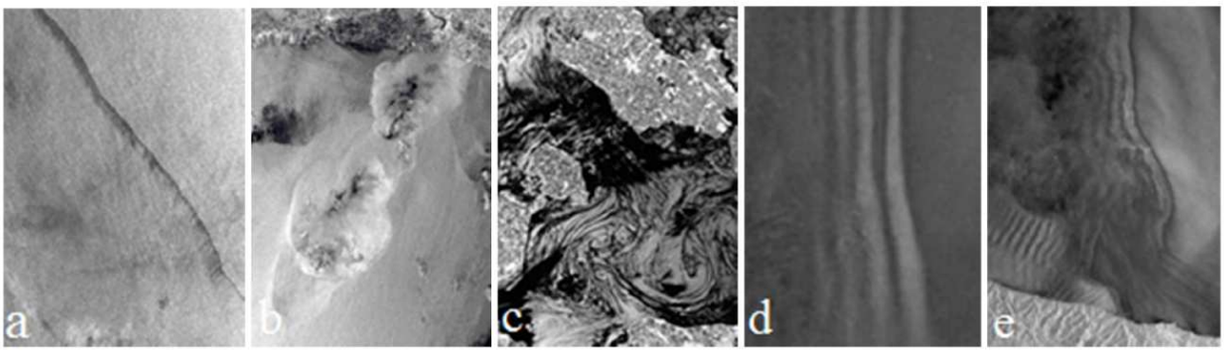

Figure 2. Examples of several main look-alikes in SAR images: a) typical oil (Photo: Alpers et al. 2004a); b) rain cell (Photo: ESA); c) biogenic slicks (Photo: Alpers et al. 2004a); d) OIW (Photo: Alpers et al. 2011); e) AGW (Photo: Alpers et al. 2011).

As the result, in operation it is very necessary to identify real oil slicks and look-alikes in SAR images based on comprehensive analysis of their different characteristics. Compared with manual inspection, automatic or semi-automatic techniques yield better efficiency and stability, hence they have been extensively studied in recent years. The standard framework of oil-spill detection algorithms is shown in figure 3, which mainly includes steps of pre-processing (calibration, speckle filtering), dark spot segmentation, feature extraction, as well as classification.

Data pre-processing is a very fundamental procedure for improving the accuracy of oil-spill detection. Many SAR image products (ground range projected products) are descriptions of radar brightness of targets in the scene, with elevation antenna patterns and range spreading losses corrected but no angle compensation. So sometimes it is also important to remove the

http://dx.doi.org/10.5772/57477

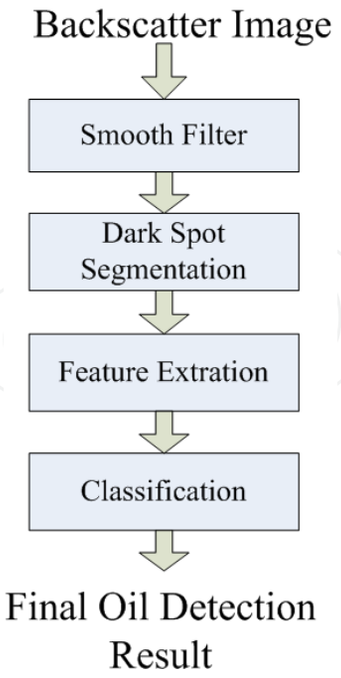

Figure 3. Flowchart of classic oil spill detection algorithms

effect of incidence angle variance before further processing (Mladenova, et al. 2013). Then images will be geo-coded to the geographical locations in the study area, for the convenience of further Geographic Information System (GIS) based study and applications.

SAR images are unavoidable suffered from speckle noise due to its coherent processing during image formation. A lot of studies have been done on segmenting dark patches that likely represent oil-slicks from the sea background. Both adapted and non-adapted threshold algorithms have been applied in dark patch detection. Solberg et al. (1999) set the threshold to k dB below the mean value of the moving window and used a multi-scale pyramid approach and clustering step in the calculation. Shu et al. (2010) made use of spatial density feature to separate dark spots and the background. Migliaccio et al. implemented oil-spill processing over single-look SAR images based on a physical model (Migliaccio et al. 2005) and used constant false alarm rate (CFAR) (Migliaccio et al., 2007a) filter to reduce the speckle within homogeneous areas without loss of information. Huang et al. (2005) used the level-set method to carry on oil-spill detection and accurately extracted oil-slicks from SAR images. However the traditional level-set methods are much more time-consuming. Zhang et al. (2012) jointly used level-set method and wavelets to provide a fast and accurate segmentation algorithm for SAR images.

In order to distinguish real oil-slicks between look-alikes, a variety features can be extracted from SAR images. Some mainly used features are listed in table 2. Polarimetric features have also been used to improve the accuracy of oil-spill classification in recent years and they will be introduced in details in the next section. It is also highly necessary to select the most suitable features for oil-slick classification. However the optimized feature sets will vary according to actual situations and also related to classification algorithm adopted.

Intensity	Morphology	Texture*	Context
Slick Backscattering (μ_{obj})			
Slick Std. Deviation (σ_{obj})	Area (A)		
Surrounding Backscattering (μ_{sce})	Perimeter (P)	Homogeneity	Distance to Coast
Intensity Ratio (μ_{obj}/μ_{sce})	Complexity (C)	Contrast	Distance to Nearest Dark
Intensity St. Dev Ratio ($\sigma_{obj}/\sigma_{sce}$)	Asymmetry	Dissimilarity	Patch
ISRI (μ_{obj}/σ_{obj})	Euler number	Entropy	Number of Surrounding
ISRO (μ_{obj}/σ_{sce})	Shape Index	Mean value	Dark Patches
Min Slick Value (MSV)	Axis Length	Std. Deviation	Number of Surrounding
Max Contrast (σ_{sce}-MSV)	Compactness	Correlation	Ships
Edge Gradient			

* Gray-Level Co-occurrence Matrix (GLCM).

Table 2. Mainly used characteristics for SAR oil-spill detection.

An example of automatic oil-spill detection using dual-threshold segmentation and characteristic possibility function is provided as follow:

The ground satellite station of CUHK received a scene of Envisat ASAR image at Hong Kong coast region on June 5th, 2007, in which several significant dark spots (Fig. 4a) can be observed. Double-threshold segmentation was firstly implemented on the received SAR data to extract both high and low levels of grayscale information from the SAR backscatter image. By using high level segmentation result, look-alikes with large area are classified from oil-spills by basic morphological analysis. By taking advantage of low threshold grayscale information, other look-alikes were distinguished from oil-spill by means of probability likelihood function derived from morphological characteristics such as complexity, length to width ratio, Euler number, etc.. Finally, the detected spills were obtained by fusing classification result of different level and other auxiliary information. The detected oil-spills are shown in Fig. 4b. From which it can be seen that using basic morphological characteristics such as complexity and length to width ratio, oil-slicks and potential look-alikes can be distinguished. However in some other cases, it is not that easy to achieve high accuracy oil-spill classification. So the studies on selecting proper characteristic as well as developing highly efficient classification algorithms are extremely important for automatic oil spill classification. And sometimes auxiliary data such as wind speed, the location of drilling platforms, ships and ship tracks, will be helpful to verify possible look-alikes.

Marghany (2001) developed a model to discriminate textures between oil and water by using co-occurrence textures. Based on Bayesian or other statistical decision, some classification algorithms were developed and applied to oil-spill detection. But the complex process of these algorithms makes it difficult to define the classification rules, since there are a lot of nonlinear and poorly understood factors in the algorithms (Topouzelis et al., 2008a; Gambardella et al., 2010). One alternative is to train the classifier using only samples of oil-spill, instead of using oil-spill and look-alikes, which is called one-class classification. Gambardella et al. (2008) proposed and used this technique with optimized feature selection algorithm and obtained

http://dx.doi.org/10.5772/57477

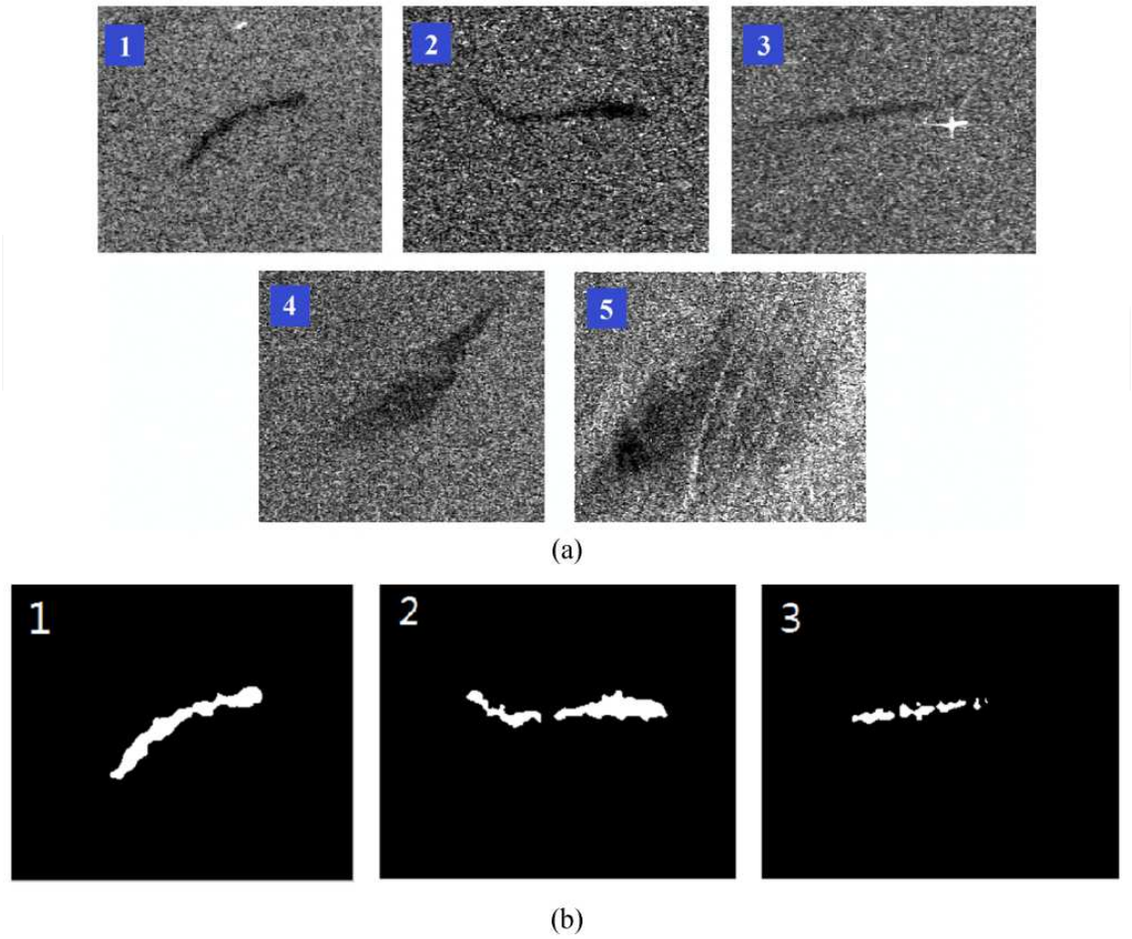

Figure 4. (a) SAR image of Hong Kong coastal region on June 5th 2007, (b) Result of automatic oil spill detection.

promising results with two case study datasets. By employing probability distribution formula, Marghany et al. (2009; 2011a) proposed fractal box counting based algorithms for oil-spill classification and further proved that this technique has promising performance in discriminating oil-spill from look-alikes on RADARSAT-1 and AIRSAR/POLSAR data.

Another alternative is taking advantage of Artificial Neural Network (ANN). Neural networks have been largely investigated and recognized as a robust tool for classification. Frate et al. (2000) proposed a semi-automatic detection of oil-spill by neural network of which the input is a vector describing features of an oil-spill candidate. It was proved that the neural network could correctly discriminate oil-spill and look-alikes over a set of independent samples. Topouzelis et al. (2007) used neural networks in both dark formation detection and oil-spill classification. During their experiment 94% of the dark formations segmentation and 89% accuracy of classification were obtained respectively. Topouzelis et al. (2009) also carried out a detailed robustness examination of the combinations derived from 25 common used features. They found that a combination of 10 features yields the most accurate results. Marghany et al. (2011b) compared three algorithms for oil-spill classification including co-occurrence textures, post supervised classification and neural network. Quantitative study on standard deviation of the estimated error shows that the artificial neural network has the largest accuracy among

all these methods. Garcia-Pineda et al. (2013) developed the Textural Classifier Neural Network Algorithm (TCNNA) to map oil-spill in Gulf of Mexico Deepwater Horizon accident by combining Envisat ASAR data and wind model outputs (CMOD5) using a combination of two neural networks. Recently, Marghany (2013) used genetic algorithm (GA) for automatic detection of oil-spill from ENVISAT ASAR data. Experimental results proved that the cross-over process and fitness function used in the study could generate accurate pattern of oil slick, and the results are shown in Fig. 5.

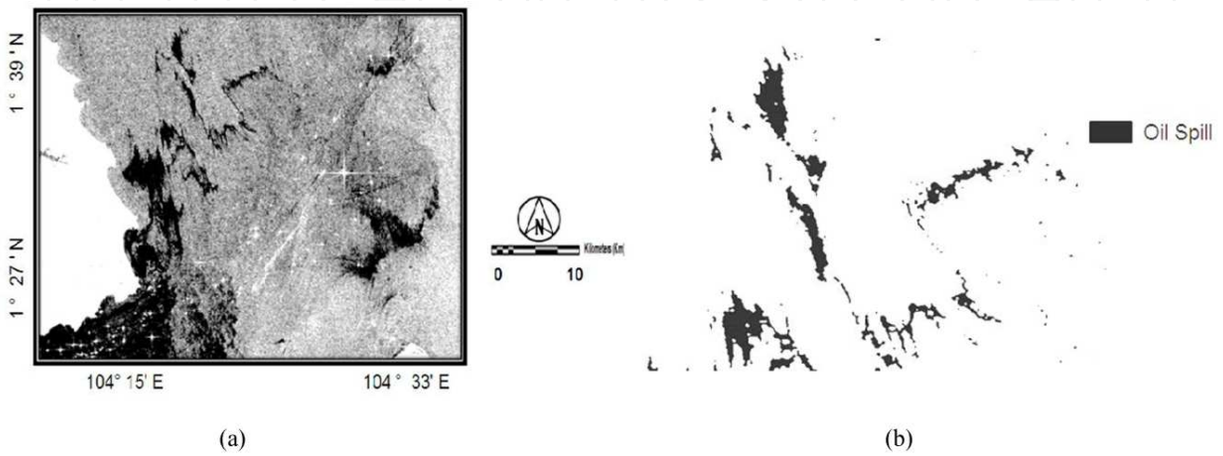

Figure 5. (a) ENVISAT ASAR data acquired on June 3rd 2010; (b) Oil spill automatic detection result by Genetic Algorithm (GA) (Marghany, 2013)

Although neural network has proven its advantage in oil-spill monitoring for SAR images, it is time consuming. Besides, the probability of misclassification does not always decrease as the number of features increases, especially when sample data is insufficient. This phenomenon is known as "the curse of dimensionality" (Jain et al., 2000). In a study (Li, et al., 2013), Support Vector Machine (SVM) was developed to automatically detect oil-spill from SAR images. A dual-threshold segmentation was implemented on SAR backscatter images to extract information in different grayscale levels. In the classification phase, a linear SVM was firstly built according to training data set. Then the constructed SVM was used to distinguish probable oil slicks and look-alikes based on morphological characteristics extracted from the dilated low threshold segmentation result. Final detection result was obtained by fusing the classification result of both low and high threshold segmentations. Experiment was carried out on two SAR images received in three days consecutively by the ground station of remote sensing satellite, CUHK. The first image received on May 19th was treated as training data sample (figure 6a). Oil-spills and look-alikes were artificaily classified and morphological features were extracted to built a SVM. The second image (figure 6b) obtained three days later was used to examine the performance of the proposed algorithm. Exparimental results illustrates that this new procedure is able to effecively detect oil-slicks, including small-size ones in coastal region based on prior morphological characteristics. In the comparation between characteristic possibility function (CPF) based method, the SVM method has better

performance in reduceing both type I (incorrect rejection) and type II (incorrect acceptance) error. And in the comparaion with ANN based methods, lower false alarm rate was obtained.

With years of study, the accrcy and efficiency of automatic oil-spill detecion and classificaion has been largely improved. However at present stage, they are not very much likely to operate fully alone without the assistance and guidance of human experts. That is because there are always some unpredicable phenomenon observed in SAR images, which is new to the sample case based automatic recognition system, calls for comprehensive analysis based on related knowledge and auxiliary data support.

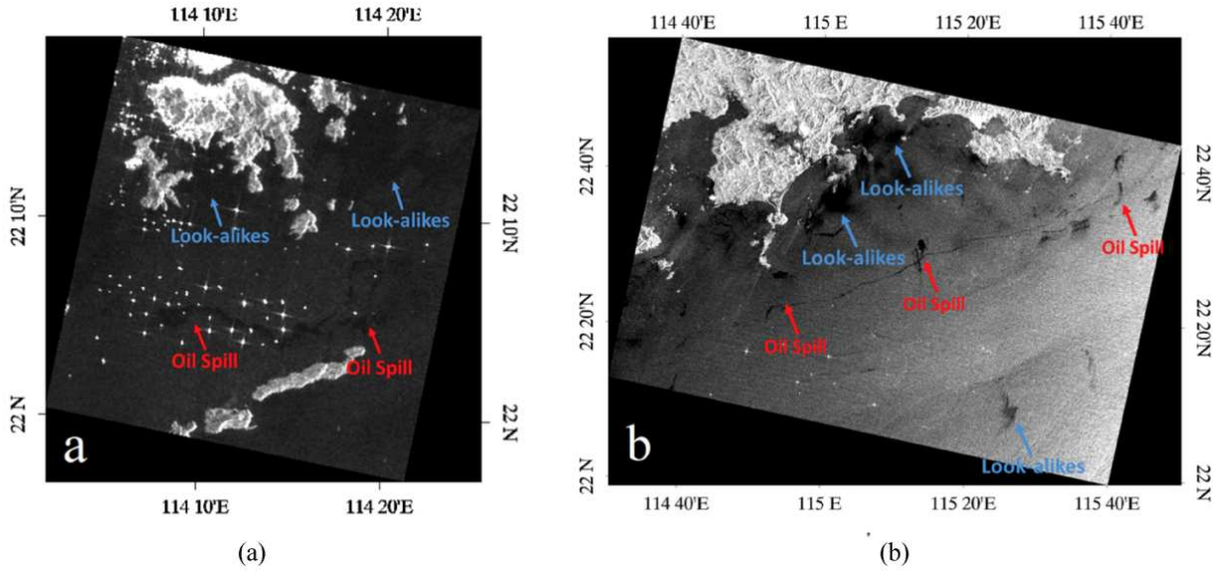

Figure 6. (a) ENVISAT ASAR image received on 10:13 a.m., May 19th 2010, Hong Kong coastal region, in which oil slicks lie in the lower middle part, along the main ship lane, so they are probably caused by deliberate discharges of ships. Look-likes are also found in the upper part of this image, where the wind are blocked by islands; (b) ENVISAT ASAR SAR image near Shanwei's coast on 10:18 a.m. 22nd May, 2010. It could be calculated that during three days the main part of the slick has drifted for almost 80 km, and it is largely stretched by the combined effect of wind and sea current. There are also several wind shelter look-alikes (upper) and look-alikes probably caused by biogenic film (lower right).

5. Trends of the studies on SAR oil-spill detection

5.1. Polarimetric SAR for oil-spill detection

Sometimes oil slicks and look-alikes can be well distinguished using above mentioned characteristics, however these characteristics of oceanic phenomenon in SAR images may vary according to specific conditions, which may results in misclassification. For example in some cases biogenic films holds very similar shape and texture as mineral oil. So the largest challenge that automatic oil-spills detection facing is to reduce the false alarm rate. Polarimetric SAR capabilities of new SAR sensors will help reduce false targets in SAR imagery (Brown and

Fingas, 2003). The feasibility of polarimetric SAR oil-spill classification relies on the fact that the polarimetric mechanisms for oil-free and oil-covered sea surface are largely different (Migliaccio et al., 2010). Before the availability of polarimetric observation, mineral oil and look-alikes such as biogenic slicks are difficult to be distinguished because they damp short gravity-capillary waves with almost the same strength (Alpers, 2002). Based on different polarimetric scattering behaviors, mineral oil and biogenic slicks can be better distinguished: for oil-covered area, Bragg scattering mechanism is largely suppressed and high polarimetric entropy can be witnessed, while in case of a biogenic slick, Bragg scattering is still dominant, but with a lower intensity. So similar polarimetric behavior as oil-free area is expected for biogenic films (Migliaccio et al., 2009). In the following part, polarimetric characteristics that may boost the performance of oil-spill detection will be listed and discussed:

i. Cross & Co-Polarization Ratio: the power ratio between HH and VV or HV and HH/VV channels. They are easy to be derived and can be obtained through dual-pol systems. In tilted Bragg scattering model adopted by Minchew et al. (2012a), they are only functions of dielectric constant and incidence angle. However actual situations are always more complicated and further study is needed. Co-polarization ratio was also proved to be possible to discriminate slicks from look-alike features associated with low-wind conditions and surface current effects (Kudryavtsev et al., 2013).

ii. Pedestal Height: describes the polarization signature. It was tested on L-band ALOS-PALSAR, C-band RADARSAT-2 and C-band SIR-C/X-SAR full-polarimetric SAR data to distinguish oil slicks from weak-damping look-alikes (Nunziata et al. 2011).

iii. Co-Polarized Phase Difference (CPD): describes the complex correlation between HH and VV channel signal. Migliaccio et al. (2009) firstly used the standard deviation of CPD to distinguish oil slicks and biogenic slicks and also pointed out that theoretically it performs better in C-band rather than L-band or lower wavelength.

iv. Degree of Polarization (DOP): a fundamental characteristic of partially polarized EM field (Shirvany, et al. 2012) derived from stokes parameters. It can take the advantage of full-pol, compact or linear dual polarization SAR data and has proven its effectiveness on oil-spill detection by Radarsat-2 and UAVSAR L-band data.

v. Pauli Decomposition Parameters: Entropy H, Anisotropy A, Alpha angle α, Alternative Entropy A_{12} and λ_i (i=1, 2, 3), they are very important parameters in almost all polarimetric analysis. Based on SIR-C/X SAR data, the performance of H and A was validated (Migliaccio et al., 2005). Then a polarimetric constant false alarm rate filter was developed to detect oil slicks over SAR images (Migliaccio et al., 2007b).

vi. Conformity Coefficient: an indicator of Bragg scattering (Zhang et al., 2011). It was tested using RADARSAT-2 quad-polarization SAR image of oil slicks in the Gulf of Mexico.

vii. Bragg Likelihood Ratio: Based on the same principle as CPD, Salberg et al. (2012) developed a generalized likelihood ratio test to see whether the Bragg scattering model is followed.

http://dx.doi.org/10.5772/57477

Some of the above mentioned polarimetric characteristics are tested by L-band UAVSAR data obtained during the Gulf of Mexico Deep Water Horizon oil-spill accident. It is noted that for different bands, environmental conditions and types, status of leaked oil, their polarimetric characteristic may be different. Nevertheless with the help of polarimetric information, scattering mechanism of sea surface can be better identified and more accurate classification result could be obtained.

The different polarimetric characteristics obtained by the observation of L-band UAVSAR, in case of DWH oil-spill accident can be perceived from figure 7. Within these parameters: co- and cross-polarization ratio, Degree of Polarization, Entropy H, Alpha angle α, Anisotropy A (within certain incidence angle range), works relatively better in distinguishing oil and sea water; while the Co-polarized phase difference, Conformity coefficient, Co-pol correlation coefficient, less work. Actually according to the discussion in Migliaccio et al (2009), CPD in L-band SAR does not perform well in the classification between mineral and biogenic oil films. Besides, Pol-SAR characteristics are observed varies with incidence angle. It has to be noted that the DWH oil-spill is a very rare case for its extreme amount of oil leaked, so actually the sea is "full" of oil and as first approximation it is possible to consider the scattering surface as a homogeneous and thick oil layer.

Analysis was conducted by Minchew et al. on the same dataset (Minchew, 2012a), in which it is also found that the major eigenvalue λ_1 of oil covered area is constantly lower than that of clean water, making it a very good indicator for oil-spill. The study also highlighted the effect of the noise floor of the radar system to the polarimetric characteristics, especially those closely related to cross-channel signal. Systematic errors such as cross-talk, channel imbalance and thermal noise largely affects this dataset, which is also one of the reason that some polarimetric characteristics various so much from near to far incidence angle. More precise calibration is required if higher classification accuracy is expected by using this UAVSAR dataset.

Similar study was conducted by Skrunes et. al (2012) during the Norwegian oil-on-water experiment, in which Radarsat-2 C-band and TerraSAR-X X-band data was used. The largest difference in findings between Skrunes' experiment and the above analysis is that for C and X band, CPD and correlation magnitude works well in the classification between mineral and biogenic oil.

Moreover, because of the complexity of sea surface polarimetric scattering mechanisms, it is unrealistic to consider using one single characteristic to distinguish variety kinds of oil-spill under different conditions. As the result, a synthetic and proper use of the aforementioned or other polarimetric characteristics is the key to accurate detection and successful interpretation of oil slicks.

5.2. Compact polarimetric SAR for oil-spill detection

Although being proved helpful in oil-spill classification, full polarimetric SAR is facing the challenges of system complexity and reduced swath width caused by doubled Pulse Repetition Frequency. Compact polarimetric (CP) modes have the advantage of un-halved swath width and comparable polarimetric capabilities compared with full polarimetric mode, which has

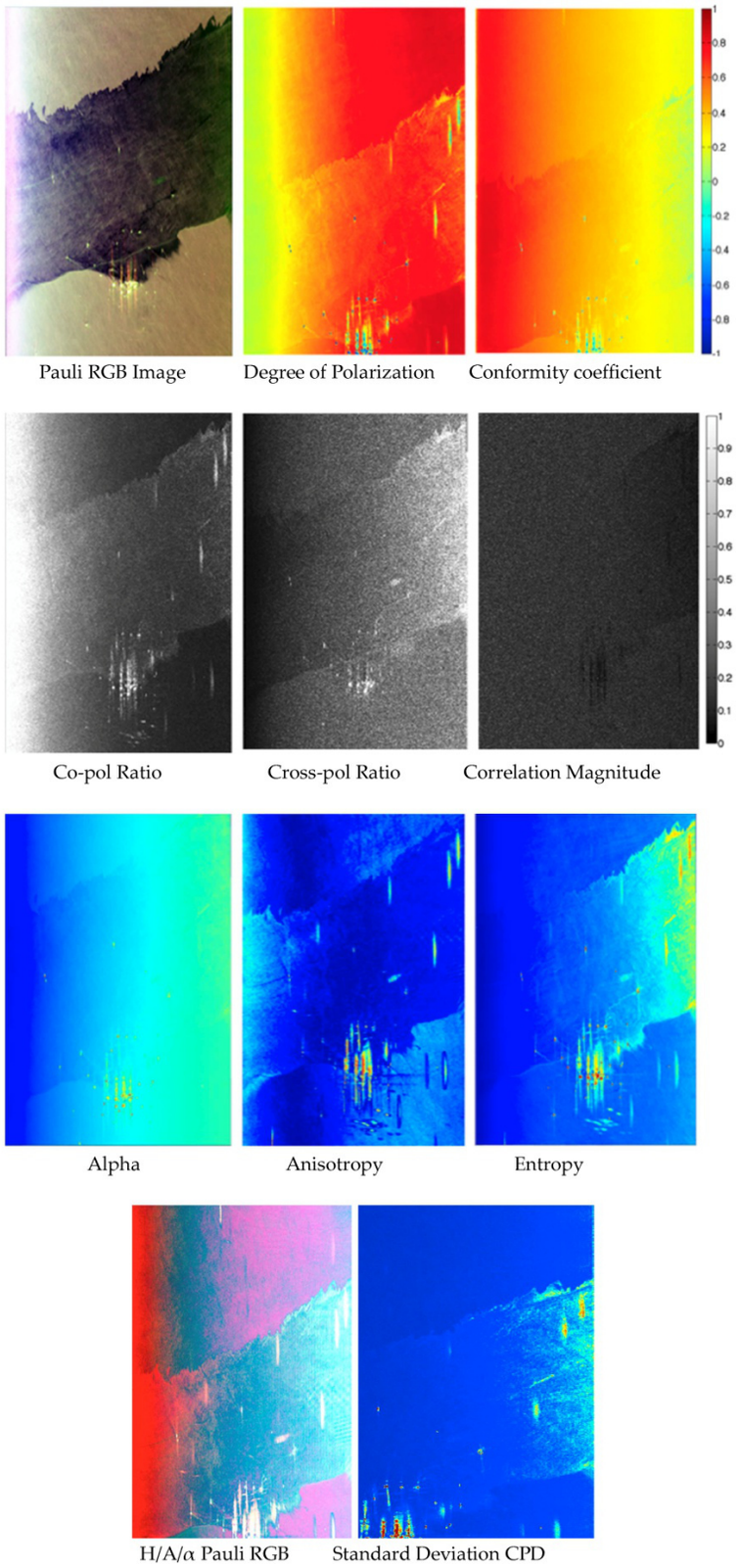

Figure 7. Polarimetric characteristics of DWH oil-spill: the horizontal direction in SAR images is accordance with range direction from the sight of the sensor, and vertical side stands for azimuth direction.

http://dx.doi.org/10.5772/57477

become a new study trend (Souyris et al., 2005; Chen et al., 2011; Nord et al., 2009). In the consecutive years after this technique was proposed, most of the studies were on its applications of land monitoring, e.g., biomass and soil moisture estimation (Dubois-Fernandez et al., 2008). Until recent years, it has been considered in maritime surveillance applications (Yin et al., 2011; Collins et al., 2013) but there are very few studies on oil-spill detection using CP SAR. Actually for sea surface the scattering mechanisms are relatively simpler than that of ground surface, so it is easier to extract and analyze useful information from CP SAR data of sea surface.

In case of fully-polarized SAR data, the backscattering properties of an object under certain condition can be described through a backscattering matrix as:

$$S = \begin{pmatrix} S_{HH} & S_{HV} \\ S_{HV} & S_{VV} \end{pmatrix} \tag{3}$$

where S_{xy} is the complex backscattering coefficient, with x denoting the received wave polarization and y indicating the transmitted wave polarization.

In the compact polarimetric SAR modes, the radar transmits only linear combination of horizontal and vertical ($\pi/4$) or circularly (CTLR, DCP) polarized signal and linearly (CTLR, $\pi/4$) or circularly (DCP) receives both horizontal and vertical polarizations. The 2-D measurement vector $\vec{K}$ is the projection of the full backscattering matrix on the transmit polarization state. The measurement vector $\vec{K}$ of three main compact polarimetric SAR modes can be defined as:

$$\vec{k}_{\pi/4} = [S_{\mathrm{HH}} + S_{\mathrm{HV}} \; S_{\mathrm{VV}} + S_{\mathrm{HV}}]^T / \sqrt{2} \tag{4}$$

$$\vec{k}_{\mathrm{CTLR}} = [S_{\mathrm{HH}} - iS_{\mathrm{HV}} \quad -iS_{\mathrm{VV}} + S_{\mathrm{HV}}]^T / \sqrt{2} \tag{5}$$

$$\vec{k}_{\mathrm{DCP}} = [S_{\mathrm{HH}} - S_{\mathrm{VV}} + i2S_{\mathrm{HV}} \quad i(S_{\mathrm{HH}} + S_{\mathrm{VV}})]^T / 2 \tag{6}$$

In the data received via CP SAR modes, only part of the polarimetric information is preserved. There are basically two ways to take advantage of CP SAR data. The first one is directly extract and analysis some properties from CP SAR data. Stokes parameters can be calculated in CTLR mode and further polarimetric analysis can be employed (Ranny, 2007). Then some important polarimetric parameters such as DOP, Relative Phase, Entropy, Anisotropy and α can be derived (Shirvany, et al., 2012; Cloude, et al., 2012). It is noted that the processing method and definitions of some parameters for CP SAR data, in the process of calibration, decomposition and classification, will be different.

The other way is to reconstruct quad-polarimetric matrix from CP SAR data. In order to reconstruct the quad-pol data from the compact polarimetric SAR data using iteration based algorithm, Souyris et al. linked the magnitude of linear coherence and the cross polarization ratio with parameter N (Souyris et al., 2005). Nord modified Souyris' algorithm by replace N

with ($|S_{HH} - S_{VV}|^2 / |S_{HV}|^2$), and update it during the calculation process iteratively (Nord et al. 2009). Yin et al. proposed a reconstruction algorithm based on polarimetric decomposition and proved its soundness in ships detection (Yin et al. 2011). Collins proposed an empirical model to estimate N in variance of incidence angles by fitting the observed data with negative exponent function (Collins et al. 2013).

Experiments on JPL-UAVSAR data can be taken to illustrate the feasibility of quad-pol reconstruction with compact polarimetric SAR modes (Li et al., 2013). Compact polarimetric SAR signals are derived from full polarimetric SAR matrix of UAVSAR data. Then Souyris' quad-pol reconstruction algorithms were employed with a slightly modified hypothetical function, to better fit the character of sea surface scattering:

$$\frac{\langle |S_{HV}|^2 \rangle}{\langle |S_{HH}|^2 \rangle + \langle |S_{VV}|^2 \rangle} = \frac{1 - |\rho_{HHVV}|}{N} \tag{7}$$

Then by using iterative algorithms, quad-pol SAR image can be reconstructed. We are not going to repeat the iterative quad-pol reconstruction algorithms here, readers who are interested may refer to papers of Souyris et al., (2005), Nord et al., (2009) and Li et al. (2013). From visual inspection, it can be found that the reconstructed quad-pol image from CP data is highly similar with the pseudo color image of the original FP data. Based on quantitative analysis, it is found that for HH and VV channel, the reconstruction accuracy are much higher in both statistical and information theoretical analysis than HV channel. The reason is that due to the dominant Bragg scattering on the sea surface, the cross-pol return is much lower than the co-pol channels. Then some polarimetric characteristics such as co-and cross-polarization ratio, standard deviation of CPD, can be estimated from the reconstructed quad-pol image, to improve the accuracy of oil-spill classification.

5.3. Oil properties retrieve

For higher level applications of SAR oil-spill remote sensing, obtaining the location and coverage of oil-spill is definitely far from enough. It is also crucial to identify oil types for estimating its potential harm to ecosystem and arranging proper cleanup methods.

Although the terminology used to describe oil-spill is not always consistent, NOAA has developed a general glossary of terms to describe the thickness and mixture status of oil floating on the sea water (NOAA, 1996), by which oil slicks can be roughly classified into Light Sheen, Silver Sheen, Rainbow Sheen, Brown oil, Mousse, Black oil, Streamers, Tarballs, Tarmats and Pancakes.

Simply by SAR remote sensing, detailed parameters of oil-spill used to be hard to obtain due to complicated sea surface status and low interaction of oil film with microwave. Among these parameters, dielectric constant (permittivity) is a key one. It describes the material's capability of holding electro-magnetic energy or polarization, which is helpful in identifying the types and conditions of the oil. During BP Deepwater Horizon oil-spill accident, oil-spill were observed by UAVSAR (Minchew, et. al, 2012a; 2012b). Because of the extreme amount of oil

leakage (approximately 700,000 m^3), the thickness of oil film/emulsion is sufficient to significantly affect the permittivity of sea surface at frequency of L-band (with wave length of approximately 24cm). Based on tilted Bragg scattering theory, the effect of oil on the dielectric permittivity and roughness spectrum was separated. It is worth noting that the DWH accident is very special for its large amount and deep source of leakage. On the way to sea surface crude oil was naturally refined and mixed with sea water, formed very complicated mixture, e.g., emulsion. So in that case, L-band SAR could observe the change of permittivity. Unfortunately in most other cases the situation is largely different.

Two-scale Boundary Perturbation Method (BPM) scattering model was used to analyze sea surface with and without biogenic slicks (Nunziata, et al., 2009). The model has the advantage of considering both large-scale sea roughness and the small-scale wave superposed on it. Compared with untitled SPM approach, the Two-scale BPM contrast model is much more accordance with the actual behavior of microwave sea surface scattering, and will be a very powerful tool for the future study. More studies are hence needed on the modeling of oil weakened sea scattering and dielectric constant of mixed oil and sea water.

The thickness of the oil slick provides vital information for estimating the amount of the spill and forecast its dispersing (Kasilingam, 1995). Near-infrared and color sensors such as MERIS and MODIS are considered to be very suitable for retrieving the thickness of oil films (Carolis et al., 2012). Hyperspectral signature is also proved to be adequate (Cong et al., 2012). However although theoretically possible, there aren't many soundness methods for retrieving oil thickness by SAR. In 1990s, polarimetric radar signature was firstly considered to estimate the thickness of thin oil films (Kasilingam, 1995). Recently Ivanova is trying to use Radar Imaging Model to obtain the thickness of the oil film from 0.37 to 0.45mm on the sea surface using satellite data.

6. The environmental impact study of oil-spill pollution

Oil-spill is considered as one of the most devastating marine pollutions, which have serious influence on coastal environment (Ventikos & Psaraftis, 2004). It damages costal ecosystem in several aspects, including: biomass production, biotope landscape, greenhouse gas regulation and nutrient cycling (Mei & Yin, 2009). The environmental impact of oil pollutions depends on the type and amount of oil as well as the sensitivity of living organisms in the polluted area (Gauthier et al., 2007). As the result, the coastal data should be analyzed in order to determine to what degree oil-spill in coastal waters and their probable trajectories will influence coastal environment.

One clue of current researches is investigating how oil-spill contamination affects marine phytoplankton. A study proved that oil increase phytoplankton boom by providing surplus organic nutrient or reducing the amount of predators (Pan & Tang et al., 2011; 2012). The study concentrated on temporal variations of key phytoplankton biomass indicator: chlorophyll *a* before and after different oil-spill occurrence period. Although not much, SAR has been reported possible to observe phytoplankton blooms. For example ERS-1 observed low

backscatter areas caused by the accumulation of biological surfactants released by the plankton blooms (Svejkovsky et al., 2001). Since observation of phytoplankton blooms by SAR requires relatively strict conditions such as surface wind and incidence angle, at present stage it has better to be considered as complementary method of ocean color or radiometer observations.

Another example is the ecosystem impact study of Deepwater Horizon oil-spill based on JPL-UAVSAR data (Jones et al., 2011), in which the intrusion of oil pollution to wetlands in Barataria Bay is investigated using the polarimetric SAR data and its effect on wetland vegetation and costal algae boom is analyzed. This study proves that with fine-resolution polarimetric SAR, the damage caused by oil pollution to the coastal environment can be evaluated and the recovery of ecosystem can be tracked.

7. Conclusions

According to previous introduction and analysis, the following conclusions can be drawled: first, extraction of dark spots is a very fundamental step that calls for the physical understanding of imaging mechanisms of SAR. Second, effective and robust pattern recognition algorithms should be further developed to distinguish oil slicks from look-alikes. With the development of SAR technology, polarimetric properties have been used for target classification more frequently, and can be one of the key techniques to boost the accuracy of oil-spill classification. Moreover, compact polarimetric SAR modes have great potential in future applications, especially marine oil-spill surveillance that require large coverage area and short revisit time. Detailed properties of oil slicks at present is hard to be retrieved by SAR sensors alone, which required sophisticated damping model, refined scattering functions and high SNR SAR data. Last but not least, oil-spill has huge affection on marine environment, especially coastal zone. As a result, the study on its impact to the marine ecology is in urgent demand and calls for the common attention of scholars all over the world.

Due to the complexity of ocean physical processes, oil-spill detection by SAR is not an easy task, which calls for close cooperation between remote sensing scientists, oceanographers and electronic engineers. It is definitely not just a matter of image processing or pattern recognition. The understanding electro-magnetic behavior of oil presented sea surface is the key to understand the whole process, without which reliable and satisfactory results will never be obtained.

At last, it is worth noting that in operational oil pollution monitoring, the most cost-effective way is to take advantage of satellite-based SAR and aircraft surveillance jointly (Solberg, 2012). The former technique has unique advantage of large coverage area and all whether all day capabilities while the latter is helpful in further verification of oil-spill and collect evidence to prosecute the polluter.

Acknowledgements

This research was jointly supported by the National Science Foundation of China (41271434), GRF (CUHK457212), ITF (GHP/002/11GD), the National Key Technologies R&D Program in the 12th Five Year Plan of China (Applied Remote Sensing Monitoring System for Water Quality and Quantity in Guangdong, Hong Kong and Macau, 2012BAH32B01 & 2012BAH32B03), and the funding of Shenzhen Municipal Science and Technology Innovation Council (JCYJ20120619151239947). And the author would like to thank JPL, NASA for providing the UAVSAR data.

Author details

Yuanzhi Zhang[1,2], Yu Li[1] and Hui Lin[1,3]

1 Institute of Space and Earth Information Science & Shenzhen Research Institute, The Chinese University of Hong Kong, Hong Kong & Shenzhen, China

2 National Astronomical Observatories, Chinese Academy of Sciences, Beijing, China

3 Department of Geography and Resource Management, The Chinese University of Hong Kong, Hong Kong

References

[1] Alpers, W. (2002), Remote sensing of oil spills, Proceedings of the symposium "Maritime Disaster Management", King Fahd University of Petroleum and Minerals, Dhahran, Saudi Arabia, pp. 19-23.

[2] Alpers W., & H. Espedal (2004a). Oils and surfactants. *In "Synthetic Aperture Radar Marine User's Manual"*, US Department of Commerce: Washington, DC, pp. 263-275.

[3] Alpers, W., and Ch. Melsheimer: Rainfall (2004b), *In "Synthetic Aperture Radar Marine User's Manual, National Oceanic and Atmospheric Administration, Center for Satellite Application and Research, NOAA/NESDIS*, Washington, D.C., USA, ISBN 0-16-073214-X, pp. 355-371.

[4] Alpers, W., and W. Huang (2011), On the discrimination of radar signatures of atmospheric gravity waves and oceanic internal waves on synthetic aperture radar images of the sea surface, *IEEE Trans. Geosci. Rem. Sens.*, vol. 49, no. 3, pp. 1114-1126.

[5] Brown, C. E., & M. F. Fingas (2003), Synthetic Aperture Radar Sensors: Viable for Marine Oil Spill Response. *Proc. of 26th Arctic and Marine Oil spill Program (AMOP),* Canada.

[6] Carolis G., Adamo M., Pasquariello G. (2012). Thickness estimation of marine oil slicks with near-infrared MERIS and MODIS imagery: The Lebanon oil spill case study, *Geoscience and Remote Sensing Symposium (IGARSS), IEEE International*, pp. 3002-3005.

[7] Chen J., Quegan S. (2011). Calibration of Spaceborne CTLR Compact Polarimetric Low-Frequency SAR Using Mixed Radar Calibrators, *Geoscience and Remote Sensing, IEEE Transactions on*, vol.49, no.7, pp.2712,2723.

[8] Cloude, S. R., Goodenough, D. G., Chen, H. (2012). Compact Decomposition Theory, *Geoscience and Remote Sensing Letters, IEEE*, vol.9, no.1, pp.28-32.

[9] Collins, M. J., Denbina, M., Atteia, G. (2013). On the Reconstruction of Quad-Pol SAR Data From Compact Polarimetry Data For Ocean Target Detection, *Geoscience and Remote Sensing, IEEE Transactions on*, vol.51, no.1, pp.591-600.

[10] Dubois-Fernandez, P. C., Souyris, J-C, Angelliaume, S., Garestier, F. (2008). The Compact Polarimetry Alternative for Spaceborne SAR at Low Frequency, *Geoscience and Remote Sensing, IEEE Transactions on*, vol.46, no.10, pp.3208-3222.

[11] Frate F., Petrocchi A., Lichtenegger J.& Calabresi G. (2000). Neural Networks for Oil Spill Detection Using ERS-SAR Data. *IEEE Transactions on Geoscience and Remote Sensing*, vol. 38, no. 5, pp. 2282-2287.

[12] Gade, M. & W. Alpers (1999). Using ERS-2 SAR for routine observation of marine pollution in European coastal waters, Sci. Total Environ., vol. 237, pp. 38441-38448.

[13] Gambardella, A., Giacinto, G., Migliaccio, M. (2008). On the Mathematical Formulation of the SAR Oil-Spill Observation Problem, *Geoscience and Remote Sensing Symposium, IGARSS IEEE International*, vol.3, pp.III-1382,III – 1385.

[14] Garcia-Pineda O., MacDonald I. R., Li X., Jackson C. R., Pichel W.G. (2013). Oil Spill Mapping and Measurement in the Gulf of Mexico With Textural Classifier Neural Network Algorithm (TCNNA), *Selected Topics in Applied Earth Observations and Remote Sensing, IEEE Journal of*, no.99, pp.1-9.

[15] Gauthier M., Weir L., Ou Z., Arkett M., and Abreu R. (2007). Integrated satellite tracking of pollution: A new operational program, *in Proc. Int. Geosci. Remote Sens. Symp.*, pp. 967–970.

[16] Huang B., Li H., & Huang X. (2005). A Level Set method for Oil Slick Segmentation in SAR Images. *Int. J. Remote Sens*., vol. 26, pp. 1145-1156.

[17] Jain A. K., R. P. W. Duin, J. Mao. (2000). Statistical Pattern Recognition: A Review. *IEEE Trans. On Pattern Analysis and Machine Intelligence,* vol. 22, no. 1, pp. 4-37, Jan. 2000.

[18] Jones, C. E., B. Minchew, B. Holt, and S. Hensley (2011). Studies of the Deepwater Horizon oil spill with the UAVSAR radar, in Monitoring and Modeling the Deepwater Horizon Oil Spill: A Record-Breaking Enterprise, *Geophys. Monogr. Ser*., vol. 195, edited by Y. Liu et al., pp. 33–50, AGU, Washington, D. C.

[19] Kasilingam D. (1995). Polarimetric radar signatures of oil slicks for measuring slick thickness, Combined Optical-Microwave Earth and Atmosphere Sensing. *Conference Proceedings., Second Topical Symposium on*, pp. 3-6.

[20] Kudryavtsev, V. N., Chapron, B., Myasoedov, A. G., Collard, F., Johannessen, J. A. (2013), On Dual Co-Polarized SAR Measurements of the Ocean Surface, *Geoscience and Remote Sensing Letters, IEEE,* IEEE, vol.10, no.4, pp.761-765.

[21] Li Y., Zhang Y. (2013), Synthetic aperture radar oil spill detection based on morphological characteristics, *Geo-spatial Information Science*, to be published.

[22] Li, Y., Zhang, Y., Chen, J., Zhang, H. (2014), Improved Compact Polarimetric SAR Quad-Pol Reconstruction Algorithm for Oil Spill Detection, *Geoscience and Remote Sensing Letters*, *IEEE*, vol. 11, no.6, pp. 1139-1142.

[23] Lin C., Nutter, B., Liang D. (2012). Estimation of oil thickness and aging from hyperspectral signature, Image Analysis and Interpretation (SSIAI), *IEEE Southwest Symposium on*, pp.213-216.

[24] Marangoni, C. (1872). Sul principio della viscosith superficiale dei liquidi stabili, *Nuovo Cimento*, Ser. 2, 5/6, 239-273.

[25] Marghany, M. (2001). RADARSAT automatic algorithms for detecting coastal oil spill pollution. *International Journal of Applied Earth Observation and Geo-information*. vol. 3, iss. 2, pp. 191-196.

[26] Marghany M. and Hashim M. (2011). Comparison between Mahalanobis classification and neural network for oil spill detection using RADARSAT-1 SAR data. *International Journal of the Physical Sciences*. vol. 6 (3), pp. 566 – 576.

[27] Marghany M., Cracknell A. and Hashim M. (2009). Modification of Fractal Algorithm for Oil Spill detection from RADARSAT-1 SAR data. *International Journal of Applied Earth Observation and Geoinformation*. vol. 11, pp.96-102.

[28] Marghany M.and Hashim M. (2011a). Discrimination between oil spill and look-alike using fractal dimension algorithm from RADARSAT-1 SAR and AIRSAR/POLSAR data. *International Journal of the Physical Sciences.*

[29] Marghany, M., & M. Hashim (2011b). Comparative Algorithms for Oil Spill Automatic Detection Using Multimode RADARSAT-1 SAR Data. *IEEE International Geoscience and Remote Sensing Symposium*, pp. 2173-2176.

[30] Marghany M. (2013). Genetic Algorithm for Oil Spill Automatic Detection from Envisat Satellite Data. Edited by Misra S., Carlini M., Carmelo M. Torre, H. Nguyen, D. Taniar, Bernady O. Apduhan, and Osvaldo Gervasi, In Beniamino Murgante, *Computational Science and Its Applications – ICCSA* 2013, vol. 7972, pp 587-598.

[31] Migliaccio M., Tranfaglia M., Ermakov S. A. (2005). A Physical Approach for the Observation of Oil Spills in SAR Images. *IEEE Journal of Oceanic Engineering*, vol. 30, no. 3., pp. 496-507.

[32] Migliaccio, M. (2010). Pedestal height for sea oil slick observation, *Radar, Sonar & Navigation, IET*, vol 5, no. 2, 103-110.

[33] Migliaccio, M., F. Nunziata, & A. Gambardella (2009). On the co-polarized phase difference for oil spill observation. *Interl. J. Remote Sens*., vol. 30, 1587-1602.

[34] Migliaccio, M., G. Ferrara, A. Gambardella, & F. Nunziata (2007a). A new stochastic model for oil spill observation by means of single-look SAR data. Environ. *Res. Eng. Manag*., vol. 39, pp. 24-29.

[35] Migliaccio, M., Gambardella, A.; Tranfaglia, M. (2007b). SAR Polarimetry to Observe Oil Spills, *Geoscience and Remote Sensing, IEEE Transactions on*, vol. 45, no. 2, pp. 506-511.

[36] Migliaccio, M., Tranfaglia, M. (2005). A study on the use of SAR polarimetric data to observe oil spills, *Oceans 2005-Europe*, vol. 1, pp.196-200.

[37] Minchew, B., Jones, C.E., Holt, B. (2012a). Polarimetric Analysis of Backscatter From the Deepwater Horizon Oil Spill Using L-Band Synthetic Aperture Radar, *Geoscience and Remote Sensing, IEEE Transactions on*, vol.50, no.10, pp.3812-3830.

[38] Minchew, B. (2012b). Determining the Mixing of Oil and Sea Water Using Polarimetric Synthetic Aperture Radar, Geophys. Res. Lett,, in press.

[39] Mladenova, I. E., Jackson, T. J.; Bindlish, R., Hensley, S. (2013). Incidence Angle Normalization of Radar Backscatter Data, Geoscience and Remote Sensing, IEEE Transactions on, vol. 51, no. 3, pp.1791-1804.

[40] NOAA (1996). Aerial observations of oil at sea, Office of Ocean Resources Conservation and Assessment.(http://docs.lib.noaa.gov/rescue/NOAA_E_DOCS/E_Library/ORR/oilspills/OilatSea.pdf).

[41] Nord, M. E., Ainsworth, T.L., Jong-Sen Lee, Stacy, N. J. S. (2009). Comparison of Compact Polarimetric Synthetic Aperture Radar Modes, *Geoscience and Remote Sensing, IEEE Transactions on*, vol.47, no.1, pp.174-188.

[42] Nunziata, F., Gambardella, A., Migliaccio, M. (2008). On the Use of Dual-Polarized SAR Data for Oil Spill Observation, *Geoscience and Remote Sensing Symposium, IEEE International*, vol.2, pp.II-225,II-228, pp. 7-11.

[43] Nunziata, F., Migliaccio, M. (2011). Gambardella, A.. Pedestal height for sea oil slick observation, *Radar, Sonar & Navigation, IET,* vol. 5, no. 2, pp.103-110.

[44] Nunziata, F.; Sobieski, P.; Migliaccio, M. (2009), The Two-Scale BPM Scattering Model for Sea Biogenic Slicks Contrast, *Geoscience and Remote Sensing, IEEE Transactions on*, vol.47, no.7, pp.1949-1956.

[45] Pan, G., Tang, D., Zhang, Y. (2012). Satellite monitoring of phytoplankton in the East Mediterranean Sea after the 2006 Lebanon oil spill. *International journal of remote sensing*, 33(23), pp. 7482-7490.

[46] Raney, R. K. (2007). Hybrid-Polarity SAR Architecture, *Geoscience and Remote Sensing, IEEE Transactions on*, vol.45, no.11, pp.3397-3404.

[47] Salberg, A.-B.; Rudjord, O.; Solberg, A.H.S. (2012). "Model based oil spill detection using polarimetric SAR," *Geoscience and Remote Sensing Symposium (IGARSS), IEEE International*, pp.5884-5887.

[48] Shirvany, R., Chabert, M., Tourneret, J.-Y. (2012). Ship and Oil-Spill Detection Using the Degree of Polarization in Linear and Hybrid/Compact Dual-Pol SAR, *Selected Topics in Applied Earth Observations and Remote Sensing, IEEE Journal of*, vol. 5, no. 3, pp.885-892.

[49] Shu Y., Li J., Yousif H. (2010). Dark-spot detection from SAR intensity imagery with spatial density thresholding for oil-spill monitoring, *Remote Sensing of Environment*, vol. 114, issue 9, pp. 2026–2035.

[50] Skrunes S., Brekke C., Eltoft T. (2012), An experimental study on oil spill characterization by multi-polarization SAR, *Synthetic Aperture Radar, 2012. EUSAR. 9th European Conference on*, pp.139,142.

[51] Solberg, A. H. S. (2012). Remote Sensing of Ocean Oil-Spill Pollution, *Proceedings of the IEEE*, vol.100, no.10, pp.2931,2945.

[52] Solberg, A., Storvik, G., Solberg, R., Volden, E (1999). Automatic Detection of Oil Spills in ERS SAR Images. *IEEE Trans. Geosci. Remote Sens*., vol. 37, no. 4, pp. 1916-1924.

[53] Souyris J. C., Imbo P., Fjortoft R., Mingot, S. and Lee J.-S. (2005). Compact polarimetry based on symmetry properties of geophysical media: The $\pi/4$ mode, *IEEE Trans. Geosci. Remote Sens.*, vol. 43, no. 3, pp. 634-646.

[54] Svejkovsky J., Shandley J. (2001). Detection of offshore plankton blooms with AVHRR and SAR imagery, *International Journal of Remote Sensing*, vol. 22, iss. 2-3, pp. 4625-4633.

[55] Topouzelis K., Karathanassi V., Pavlakis P., Rokos D. (2007). Detection and discrimination between oil spills and look-alike phenomena through neural networks. *ISPRS Journal of Photogrammetry and Remote Sensing*. vol. 62, Iss. 4, pp. 264-270.

[56] Topouzelis K., Stathakis D. and Karathanassi V.. (2008a). Investigation of Genetic Algorithms Contribution to Feature Selection for Oil Spill Detection. *International Journal of Remote Sensing*, vol. 30, no. 3, pp. 611–625.

[57] Topouzelis, K., D. Stathakis, & V. Karathanassi (2009). Investigation of genetic algorithms contribution to feature selection for oil spill detection. *Intl. J..Remote Sens*., vol. 30 no. 3, pp. 611-625.

[58] Topouzelis, K., V. Karathanassi, P. Pavlakis, & D. Rokos (2008). Dark formation detection using neural network. *Intl. J. Remote Sens*., vol. 29 no. 16, pp. 4705-4720.

[59] Yin J., Yang J., Zhang X. (2011). On the ship detection performance with compact polarimetry, *Radar Conference (RADAR), IEEE*, pp.675-680, 23-27.

[60] Zhang B., Perrie W., Li X.& Pichel W., (2011). Mapping sea surface oil slicks using RADARSAT-2 quad-polarization SAR image, *Geophys. Res. Lett*., vol. 38, L10602.

[61] Zhang Y., Lin H., Liu Q., Hu J., Li X. and Yeung K. (2012). Oil-spill monitoring in the coastal waters of Hong Kong and vicinity, *Marine Geodesy*, vol, 35, pp. 93-106.